EUROPEAN ORGANIZATION FOR NUCLEAR RESEARCH

Inclusive D*± Production in Two-Photon Collisions at LEP

The L3 Collaboration

Abstract

Inclusive D*± production in two-photon collisions is studied with the L3 detector at LEP, using 683 pb^{-1} of data collected at centre-of-mass energies from 183 to 209 GeV. Differential cross sections are determined as functions of the transverse momentum and pseudorapidity of the D*± mesons in the kinematic region 1 GeV $< P_T <$ 12 GeV and $|\eta| < 1.4$. The cross sections $\sigma(\mathrm{e^+e^-} \to \mathrm{e^+e^-D^{*\pm}X})$ in this kinematical region is measured and the $\sigma(\mathrm{e^+e^-} \to \mathrm{e^+e^-c\bar{c}X})$ cross section is derived. The measurements are compared with next-to-leading order perturbative QCD calculations.

arXiv:hep-ex/0204027v1 19 Apr 2002

1 Introduction

The measurement of open charm production in two-photon collisions provides a good test of perturbative QCD as the large physical scale set by the charm quark mass is expected to make the perturbative calculations more reliable. At LEP2 energies, the direct and single resolved processes, sketched in Figure 1, are predicted [1] to give comparable contributions to the cross section $\sigma(\gamma\gamma \to c\bar{c})$. The contributions to open charm production from soft processes described by the Vector Dominance Model (VDM) and from double resolved processes are expected to be small. The resolved photon cross section is dominated by the photon-gluon fusion process $\gamma g \to c\bar{c}$. The cross section for open charm production in two-photon collisions therefore depends on the charm quark mass and on the gluonic parton density function of the photon. Measurements of open charm production in untagged two-photon collisions were performed at PEP [2], PETRA [3], TRISTAN [4], and LEP [5–8], where charm quarks were identified by the presence of $D^{*\pm}$ mesons, leptons or K^0_S mesons.

This letter describes the results of a measurement of the $e^+e^- \to e^+e^-c\bar{c}X$ cross section at centre-of-mass energies ranging from 183 to 209 GeV. The data sample corresponds to a total integrated luminosity of 683 pb^{-1} collected with the L3 detector [9] at LEP. Charm quarks are identified by reconstructing D^{*+} [1)] mesons in three decay channels:

$$D^{*+} \to D^0\pi_s^+ \to (K^-\pi^+)\pi_s^+ \tag{1}$$

$$D^{*+} \to D^0\pi_s^+ \to (K^-\pi^+\pi^0)\pi_s^+ \tag{2}$$

$$D^{*+} \to D^0\pi_s^+ \to (K^-\pi^+\pi^-\pi^+)\pi_s^+. \tag{3}$$

π_s^+ stands for a "slow pion", so called as the kinetic energy release in D^{*+} decays is only about 6 MeV. Differential cross sections for $D^{*\pm}$ production as a function of its transverse momentum P_T and pseudorapidity η are determined together with the visible cross section. This is then extrapolated to derive $\sigma(e^+e^- \to e^+e^-c\bar{c}X)$.

The PYTHIA [10] Monte Carlo program is used to model two-photon processes. It simulates $\gamma\gamma$ events according to the current knowledge of hadronic interactions obtained from pp and γp studies. Two Monte Carlo samples are used: one with massless quark matrix elements, and another with matrix elements with a charm quark mass $m_c = 1.35$ GeV. Both direct and resolved diagrams are included in the generation. The resolved processes are generated with the SaS1d photon parton density function [11]. A two-photon luminosity function corresponding to the Equivalent Photon Approximation [12] is used with a cut off $Q^2 < m_\rho^2$. The L3 detector is simulated with the GEANT package [13] and Monte Carlo events are reconstructed in the same way as the data events. Time dependent detector inefficiencies, as monitored during the data taking period, are also simulated.

2 Event Selection and $D^{*\pm}$ Reconstruction

The event selection follows two steps: first, hadronic final states from two-photon collisions are selected, then, $D^{*\pm}$ mesons are reconstructed.

[1)]Charge conjugate states are assumed to be included.

2.1 Selection of Hadronic Two-Photon Events

Hadronic events are required to contain at least four particles, with at least three charged tracks. A particle is defined as either a track in the central tracker or a calorimetric cluster not associated to a track. The background from $e^+e^- \to e^+e^-\tau^+\tau^-$ and $e^+e^- \to \tau^+\tau^-$ events is highly suppressed by this requirement. To reject annihilation events, the visible energy has to be less than 80 GeV. The analysis is restricted to events with visible mass $W_{\text{vis}} > 2$ GeV, as calculated from tracks and calorimetric clusters, including those from the small angle luminosity monitor. All particles are considered to be pions, except for unmatched electromagnetic clusters considered as photons.

An anti-tagging condition is implemented on the scattered electron or positron, by requiring the energy of the most energetic cluster in the forward electromagnetic calorimeter to be less than $0.2\sqrt{s}$. Only 6% of events in the $D^{*\pm}$ signal region are rejected by this criterium. The anti-tagging requirement implies a small virtuality of the interacting photons: $\langle Q^2 \rangle \simeq 0.1$ GeV^2, as predicted by the PYTHIA Monte Carlo.

This preselection yields 4.6×10^6 events. After applying the above cuts, the contamination from annihilation processes is less than 1%.

2.2 $D^{*\pm}$ Reconstruction

The $D^{*\pm}$ selection requires events with less than 15 tracks. Tracks are required to have at least 20 hits, a transverse momentum above 0.1 GeV and a distance of closest approach to the interaction point in the transverse plane below 1.5 mm. In addition, photon candidates are selected in the electromagnetic calorimeter as isolated showers with no close tracks. $D^{*\pm}$ mesons are selected by first identifying D^0 mesons. Additional criteria reject the combinatorial background, and finally, π_s^+ candidates are added. The D^0 candidates are reconstructed from two-track combinations for the channel (1), two-track and two-photon combinations for the channel (2), and four-track combinations for the channel (3). Pion or kaon masses are assigned to the tracks. We define P_K and P_π as the probabilities for the kaon and pion mass hypotheses, calculated from the energy loss, dE/dx, in the tracker. The joint probabilities $P_K P_\pi$ for channels (1) and (2) and $P_K P_\pi^1 P_\pi^2 P_\pi^3$ for channel (3), have to be greater than 0.5% and 0.1% respectively. In addition, for channel (3) the kaon track should satisfy the condition $P_K/P_\pi \geq 2$. The π^0 candidates for channel (2) are constructed from two neutral clusters in the barrel electromagnetic calorimeter, with energy greater than 50 MeV and effective mass within ± 20 MeV of the nominal π^0 mass. The transverse momentum of the π^0 candidate with respect to the beam direction must be greater than 400 MeV.

The effective mass of the D^0 candidate in the $K^-\pi^+$, $K^-\pi^+\pi^0$, or $K^-\pi^+\pi^-\pi^+$ combinations is calculated for channels (1), (2) and (3), respectively. This mass should be within ± 75 MeV, ± 50 MeV, or ± 40 MeV around the nominal D^0 mass, respectively. These different mass intervals are determined by the Monte Carlo D^0 mass resolution and reflect the better transverse momentum resolution for softer tracks and the high precision π^0 reconstruction in the BGO electromagnetic calorimeter.

To reduce the combinatorial background in channel (1), the opening angle α between the kaon and the D^0 flight direction has to satisfy the condition $\cos\alpha > -0.1$.

A kinematical fit using as constraints the D^0 and π^0 masses is performed for channel (2). The fit probability must be greater than 1%. In addition, the sum of the transverse momenta squared of these particles must exceed 0.9 GeV^2. Since the decay $D^0 \to K^-\pi^+\pi^0$ proceeds dominantly through one of the quasi-two-body intermediate states $\bar{K}^{*0}\pi^0$, $K^{*-}\pi^+$ and $K^-\rho^+$ [14], the $K^-\pi^+$

and $K^-\pi^0$ combinations are required to lie within ± 60 MeV of the $K^*(892)$ mass and the $\pi^-\pi^0$ ones within ± 150 MeV of the ρ mass. This last criterium also holds for channel (3), that proceeds through the $K\pi\rho$ state. In addition, for channel (2) we require the helicity angle θ^* of an intermediate decay state to satisfy the condition $|\cos\theta^*| > 0.4$, exploiting the P-wave properties of vector-particle decay into two scalar particles to reject background. The helicity angle θ^* is defined as the angle between the direction of a decay product of the vector resonance ($\bar{K}^{*0}$, K^{*-} or ρ^+) and the direction of the pseudoscalar particle (π^0, π^+ or K^-) from the D^0 decay, calculated in the intermediate resonance rest frame.

D^0 decay tracks are required to originate near the interaction point. This is enforced by reconstructing a secondary vertex in the transverse plane for channels (1) and (3). The D^0 impact parameter d with respect to the interaction point in the transverse plane must satisfy $d < 0.8$ mm and $d < 0.6$ mm respectively, while the D^0 signed flight distance s should satisfy $-0.8 < s < 1.0$ mm and $-0.9 < s < 1.1$ mm, respectively. No secondary vertex reconstruction is performed for channel (2), but the distance of closest approach of kaon and pion tracks to the interaction point in the transverse plane must be less than 1 mm.

Finally, a slow pion candidate track is added to the combination to form the $D^{*\pm}$ candidate. The charge must be opposite to that of the kaon candidate, with a distance of closest approach to the interaction point in the transverse plane less than 4.5 mm.

The mass difference ΔM of the $D^{*\pm}$ and D^0 candidates is shown in Figure 2. $D^{*\pm}$ mesons are expected to form a peak around 145.4 MeV, while combinatorial background yields a rising distribution, starting at 139.6 MeV, the mass of the charged pion. The reconstructed $D^{*\pm}$ signal is clearly observed in all the three decay channels under study. The number of observed $D^{*\pm}$ mesons is estimated by a fit to the ΔM spectrum. The background shape is modelled by Monte Carlo and checked using wrong-charge combinations in data, where the charge of the kaon candidate is the same as the charge of the slow pion candidate. The background processes $e^+e^- \rightarrow \gamma/Z \rightarrow q\bar{q}$ and $e^+e^- \rightarrow W^+W^- \rightarrow q\bar{q}q\bar{q}$ represent less than 0.2% of the sample. The background shape is modelled by a function with two free parameters a and b:

$$f_{bkg}(\Delta M) = a(\Delta M - m_\pi)^b, \tag{4}$$

where the background shape parameter b is determined from the $e^+e^- \rightarrow e^+e^-q\bar{q}$ Monte Carlo. A fit to the ΔM spectrum is performed, using a variable width Gaussian to describe the signal, and the fitted numbers of $D^{*\pm}$ mesons $N_{obs}^{D^{*\pm}}$ found in each channel are presented in Table 1.

3 Results

3.1 Differential cross sections

The measured differential cross sections for inclusive $D^{*\pm}$ production as a function of its transverse momentum P_T and pseudorapidity η, $d\sigma/dP_T$ and $d\sigma/d|\eta|$, are shown in Tables 2 and 3 for the visible region defined by:

$$1 \text{ GeV} < P_T < 12 \text{ GeV} \quad \text{and} \quad |\eta| < 1.4 . \tag{5}$$

When evaluating $d\sigma/dP_T$, which has a steep dependence on P_T, a correction factor, determined from Monte Carlo, is used to assign the differential cross sections to the centers of the corresponding bins. The selection efficiency is determined with PYTHIA, using the D^{*+} branching ratios of Reference 14 and assuming a 1 : 1 mixture [1,7] of direct and single resolved processes. The sources of systematic uncertainty are discussed below and summarised in Table 4:

- Selection procedure. The uncertainty is estimated by a variation of the selection criteria. The largest contributions are the cut on the number of tracks (6.0%) and the D^0 mass window (4.6%) for channel (1); the cut on the transverse momentum of the neutral pion (7.8%) and on the sum of transverse momenta (4.3%) for channel (2); the cut on the dE/dx probability (11.5%) and the D^0 mass window (7.5%) for channel (3).

- Branching ratios. The uncertainties are taken from Reference 14.

- Background. This uncertainty is obtained by changing the background fit function within the uncertainties on its parameters. The range of the fit is also varied.

- Ratio of the direct to resolved processes. The selection efficiency is re-evaluated changing the ratio from $1:1$ to $3:1$ or $1:3$.

- Monte Carlo statistics.

- Trigger efficiency. The trigger efficiency and its uncertainty are determined from the data using a set of independent triggers.

Figures 3 and 4 show the differential cross sections $d\sigma/dP_T$ and $d\sigma/d|\eta|$. The differential cross sections are compared to next-to-leading order (NLO) perturbative QCD calculations, based on massive matrix elements [15]. In this scheme, the charm quark is not considered to be one of the active flavours inside the photon. The Glück-Reya-Schienbein [16] photon parton density is used in the calculation. The renormalization scale, μ_R, and the factorization scale of the photon structure function, μ_F, are taken as $\mu_R = \mu_F/2 = m_T = \sqrt{p_T^2 + m_c^2}$, where p_T is the transverse momentum of the charm quark whose mass is $m_c = 1.5$ GeV. The calculations are repeated with different renormalization scales separately for the direct and single-resolved contributions as well as with different charm quark masses, in order to estimate the maximal theory prediction uncertainty. The measurements are in agreement with the NLO QCD calculations within the theoretical uncertainties.

3.2   Visible cross section

The visible $D^{*\pm}$ production cross section $\sigma(e^+e^- \to e^+e^-D^{*\pm}X)_{vis}$ is calculated in the kinematical region (5) as:

$$\sigma(e^+e^- \to e^+e^-D^{*\pm}X)_{vis} = \frac{N_{obs}^{D^{*\pm}}}{\mathcal{L}\varepsilon_{trig}\varepsilon_{vis}^{D^{*\pm}}}, \tag{6}$$

where $\mathcal{L}$ is the total integrated luminosity. The trigger efficiency ε_{trig} and the selection efficiency $\varepsilon_{vis}^{D^{*\pm}}$ are listed in Table 1 and the number of observed events in Tables 2 and 3. Results for each P_T and η bin are shown in Tables 2 and 3, while the integrated visible cross sections are given in Table 1 for each channel. Averaging over the three channels gives:

$$\sigma(e^+e^- \to e^+e^-D^{*\pm}X)_{vis} = 71.2 \pm 5.3 \pm 9.8 \text{ pb},$$

where the first uncertainty is statistical and the second is systematic.

3.3 Total cross section

The total cross section of open charm production is calculated as:

$$\sigma(e^+e^- \rightarrow e^+e^- c\bar{c}X) = \frac{\sigma(e^+e^- \rightarrow e^+e^- D^{*\pm}X)_{vis} - \sigma(e^+e^- \rightarrow e^+e^- b\bar{b}X \rightarrow D^{*\pm}X)_{vis}}{\varepsilon_{tot}^{D^{*\pm}} \, 2 \, P(c \rightarrow D^{*+})}. \qquad (7)$$

The probability of a charm quark to hadronize into a D^{*+} meson, $P(c \rightarrow D^{*+})$, is equal to 0.241 ± 0.008 [17]. The efficiency $\varepsilon_{tot}^{D^{*\pm}}$ is a correction factor to extrapolate from the visible $D^{*\pm}$ kinematical region (5) to the full phase space. It follows from the calculations of Reference 15 as $\varepsilon_{tot}^{D^{*\pm}} = 0.132 \, {}^{+0.038}_{-0.043}$. The two-photon $b\bar{b}$ production process also yields $D^{*\pm}$ mesons. The cross section of this contribution, $\sigma(e^+e^- \rightarrow e^+e^- b\bar{b}X \rightarrow D^{*\pm}X)_{vis}$, is estimated from a $e^+e^- \rightarrow e^+e^- b\bar{b}X$ Monte Carlo sample and the measured $\sigma(e^+e^- \rightarrow e^+e^- b\bar{b}X)$ cross section [8] as 1.9 ± 0.4 pb. It is subtracted and its uncertainty is included in the systematics.

The total open charm production cross section at the average centre-of-mass energy of 197 GeV is estimated to be:

$$\sigma(e^+e^- \rightarrow e^+e^- c\bar{c}X) = (1.12 \pm 0.09 \pm 0.16 \, {}^{+0.54}_{-0.25}) \times 10^3 \text{ pb}.$$

The first uncertainty is statistical and second is systematic. The third uncertainty is that on the extrapolation from the visible phase space region to the full one. It corresponds to the integration [15] of the dotted and dashed lines in Figures 3 and 4. A consistent estimate of this uncertainty is also obtained by comparing the extrapolation factors obtained using different Monte Carlo generators: the massive and massless PYTHIA samples yield extrapolation factors that differ by 24%.

The total inclusive charm production cross section as a function of the e^+e^- centre-of-mass energy is shown in Figure 5 together with our previous measurements [6, 8]. The data are compared to the NLO QCD predictions of Reference 1 for the direct process and the sum of direct and resolved processes. In this calculation, the charm quark mass is taken to be 1.3 GeV or 1.7 GeV, and the open charm threshold to be at 3.8 GeV. The resolved process is calculated using the Glück-Reya-Vogt [18] photon parton density function. The renormalization and factorization scales are taken equal to the charm quark mass. The use of the Drees-Grassie [19] parton density function results in a decrease of the cross section of 9% for $m_c = 1.3$ GeV and of 3% for $m_c = 1.7$ GeV. Changing the QCD scale from m_c to $2m_c$ decreases the predicted cross section by 30% for $m_c = 1.3$ GeV and 15% for $m_c = 1.7$ GeV.

The measured cross section is in good agreement with our previous measurements [6, 8] based on lepton tag and with the QCD expectations. The contribution of the single-resolved process is needed to describe the data.

Acknowledgements

References

[1] M. Drees *et al.*, Phys. Lett. **B 306** (1993) 371.

[2] TPC/Two-Gamma Collab., M. Alston-Garnjost *et al.*, Phys. Lett. **B 252** (1990) 499.

[3] JADE Collab., W. Bartel *et al.*, Phys. Lett. **B 184** (1987) 288.
    TASSO Collab., W. Braunschweig *et al.*, Z. Phys. **C 47** (1990) 499.

[4] TOPAZ Collab., R. Enomoto *et al.*, Phys. Lett. **B 328**, (1994) 535,
    TOPAZ Collab., R. Enomoto *et al.*, Phys. Rev. **D 50** (1994) 1879,
    TOPAZ Collab., R. Enomoto *et al.*, Phys. Lett. **B 341** (1994) 99,
    TOPAZ Collab., R. Enomoto *et al.*, Phys. Lett. **B 341** (1994) 238,
    VENUS Collab., S. Uehara *et al.*, Z. Phys. **C 63** (1994) 213,
    AMY Collab., T. Aso *et al.*, Phys. Lett. **B 363** (1995) 249,
    AMY Collab., T. Aso *et al.*, Phys. Lett. **B 381** (1996) 372.

[5] ALEPH Collab., D. Buskulic *et al.*, Phys. Lett. **B 355** (1995) 595,
    L3 Collab., M. Acciarri *et al.*, Phys. Lett. **B 467** (1999) 137,
    L3 Collab., M. Acciarri *et al.*, Phys. Lett. **B 514** (2001) 19.

[6] L3 Collab., M. Acciarri *et al.*, Phys. Lett. **B 453** (1999) 83.

[7] OPAL Collab., G. Abbiendi *et al.*, Eur. Phys. J. **C 16** (2000) 579.

[8] L3 Collab., M. Acciarri *et al.*, Phys. Lett. **B 503** (2001) 10.

[9] L3 Collab., B. Adeva *et al.*, Nucl. Instr. Meth. **A 289** (1990) 35,
    L3 Collab., O. Adriani *et al.*, Phys. Rep. **236** (1993) 1,
    M. Acciarri *et al.*, Nucl. Instr. Meth. **A 351** (1994) 300,
    M. Chemarin *et al.*, Nucl. Instr. Meth. **A 349** (1994) 345,
    I.C. Brock *et al.*, Nucl. Instr. Meth. **A 381** (1996) 236,
    G. Basti *et al.*, Nucl. Instr. Meth. **A 374** (1996) 293,
    A. Adam *et al.*, Nucl. Instr. Meth. **A 383** (1996) 342.

[10] PYTHIA version 5.722 is used.
    T. Sjöstrand, Preprint CERN-TH/7112/93 (1993), revised August 1995; Comp. Phys. Comm. **82** (1994) 74.

[11] G.A. Schuler and T. Sjöstrand, Z. Phys. **C 68** (1995) 607; Phys. Lett. **B 376** (1996) 193.

[12] V.M. Budnev et al., Phys. Rep. **15** (1974) 181.

[13] GEANT version 3.15 is used.
    R. Brun *et al.*, Preprint CERN DD/EE/84-1 (1984), revised 1987;
    the GHEISHA program, H. Fesefeldt, RWTH Aachen Report PITHA 85/2 (1985), is used to model hadronic interactions.

[14] D.E. Groom *et al.,* Review of Particle Physics, Eur. Phys. J. **C 15** (2000) 1.

[15] S. Frixione, E. Laenen and M. Krämer, Nucl. Phys. **B 571** (2000) 169; J. Phys. **G 26** (2000) 723. These calculations are repeated for the kinematical region of our measurement.

[16] M. Glück, E. Reya and I. Schienbein, Phys. Rev. **D 60** (1999) 054019.

[17] The LEP Collaborations ALEPH, DELPHI, L3, OPAL, the LEP Electroweak Working Group and the SLD Heavy Flavour and Electroweak Groups. Preprint CERN-EP/2001-021, (2001).

[18] M. Glück, E. Reya and A. Vogt, Phys. Rev. **D 46** (1992) 1973.

[19] M. Drees and K. Grassie, Z. Phys. **C 28** (1985) 451.

Author List

The L3 Collaboration:

P.Achard[20] O.Adriani[17] M.Aguilar-Benitez[24] J.Alcaraz[24,18] G.Alemanni[22] J.Allaby[18] A.Aloisio[28] M.G.Alviggi[28] H.Anderhub[46] V.P.Andreev[6,33] F.Anselmo[9] A.Arefiev[27] T.Azemoon[3] T.Aziz[10,18] P.Bagnaia[38] A.Bajo[24] G.Baksay[16] L.Baksay[25] S.V.Baldew[2] S.Banerjee[10] Sw.Banerjee[4] A.Barczyk[46,44] R.Barillère[18] P.Bartalini[22] M.Basile[9] N.Batalova[43] R.Battiston[32] A.Bay[22] F.Becattini[17] U.Becker[14] F.Behner[46] L.Bellucci[17] R.Berbeco[3] J.Berdugo[24] P.Berges[14] B.Bertucci[32] B.L.Betev[46] M.Biasini[32] M.Biglietti[28] A.Biland[46] J.J.Blaising[4] S.C.Blyth[34] G.J.Bobbink[2] A.Böhm[1] L.Boldizsar[13] B.Borgia[38] S.Bottai[17] D.Bourilkov[46] M.Bourquin[20] S.Braccini[20] J.G.Branson[40] F.Brochu[4] J.D.Burger[14] W.J.Burger[32] X.D.Cai[14] M.Capell[14] G.Cara Romeo[9] G.Carlino[28] A.Cartacci[17] J.Casaus[24] F.Cavallari[38] N.Cavallo[35] C.Cecchi[32] M.Cerrada[24] M.Chamizo[20] Y.H.Chang[48] M.Chemarin[23] A.Chen[48] G.Chen[7] G.M.Chen[7] H.F.Chen[21] H.S.Chen[7] G.Chiefari[28] L.Cifarelli[39] F.Cindolo[9] I.Clare[14] R.Clare[37] G.Coignet[4] N.Colino[24] S.Costantini[38] B.de la Cruz[24] S.Cucciarelli[32] J.A.van Dalen[30] R.de Asmundis[28] P.Déglon[20] J.Debreczeni[13] A.Degré[4] K.Deiters[44] D.della Volpe[28] E.Delmeire[20] P.Denes[36] F.DeNotaristefani[38] A.De Salvo[46] M.Diemoz[38] M.Dierckxsens[2] C.Dionisi[38] M.Dittmar[46,18] A.Doria[28] M.T.Dova[11,♯] D.Duchesneau[4] B.Echenard[20] A.Eline[18] H.El Mamouni[23] A.Engler[34] F.J.Eppling[14] A.Ewers[1] P.Extermann[20] M.A.Falagan[24] S.Falciano[38] A.Favara[31] J.Fay[23] O.Fedin[33] M.Felcini[46] T.Ferguson[34] H.Fesefeldt[1] E.Fiandrini[32] J.H.Field[20] F.Filthaut[30] P.H.Fisher[14] W.Fisher[36] I.Fisk[40] G.Forconi[14] K.Freudenreich[46] C.Furetta[26] Yu.Galaktionov[27,14] S.N.Ganguli[10] P.Garcia-Abia[5,18] M.Gataullin[31] S.Gentile[38] S.Giagu[38] Z.F.Gong[21] G.Grenier[23] O.Grimm[46] M.W.Gruenewald[1] M.Guida[39] R.van Gulik[2] V.K.Gupta[36] A.Gurtu[10] L.J.Gutay[43] D.Haas[5] R.Sh.Hakobyan[30] D.Hatzifotiadou[9] T.Hebbeker[1] A.Hervé[18] J.Hirschfelder[34] H.Hofer[46] M.Hohlmann[25] G.Holzner[46] S.R.Hou[48] Y.Hu[30] B.N.Jin[7] L.W.Jones[3] P.de Jong[2] I.Josa-Mutuberría[24] D.Käfer[1] M.Kaur[15] M.N.Kienzle-Focacci[20] J.K.Kim[42] J.Kirkby[18] W.Kittel[30] A.Klimentov[14,27] A.C.König[30] M.Kopal[43] V.Koutsenko[14,27] M.Kräber[46] R.W.Kraemer[34] W.Krenz[1] A.Krüger[45] A.Kunin[14] P.Ladron de Guevara[24] I.Laktineh[23] G.Landi[17] M.Lebeau[18] A.Lebedev[14] P.Lebrun[23] P.Lecomte[46] P.Lecoq[18] P.Le Coultre[46] J.M.Le Goff[18] R.Leiste[45] M.Levtchenko[26] P.Levtchenko[33] C.Li[21] S.Likhoded[45] C.H.Lin[48] W.T.Lin[48] F.L.Linde[2] L.Lista[28] Z.A.Liu[7] W.Lohmann[45] E.Longo[38] Y.S.Lu[7] K.Lübelsmeyer[1] C.Luci[38] L.Luminari[38] W.Lustermann[46] W.G.Ma[21] L.Malgeri[20] A.Malinin[27] C.Maña[24] D.Mangeol[30] J.Mans[36] J.P.Martin[23] F.Marzano[38] K.Mazumdar[10] R.R.McNeil[6] S.Mele[18,28] L.Merola[28] M.Meschini[17] W.J.Metzger[30] A.Mihul[12] H.Milcent[18] G.Mirabelli[38] J.Mnich[1] G.B.Mohanty[10] G.S.Muanza[23] A.J.M.Muijs[2] B.Musicar[40] M.Musy[38] S.Nagy[16] S.Natale[20] M.Napolitano[28] F.Nessi-Tedaldi[46] H.Newman[31] T.Niessen[1] A.Nisati[38] H.Nowak[45] R.Ofierzynski[46] G.Organtini[38] C.Palomares[18] D.Pandoulas[1] P.Paolucci[28] R.Paramatti[38] G.Passaleva[17] S.Patricelli[28] T.Paul[11] M.Pauluzzi[32] C.Paus[14] F.Pauss[46] M.Pedace[38] S.Pensotti[26] D.Perret-Gallix[4] B.Petersen[30] D.Piccolo[28] F.Pierella[9] M.Pioppi[32] P.A.Piroué[36] E.Pistolesi[26] V.Plyaskin[27] M.Pohl[20] V.Pojidaev[17] J.Pothier[18] D.O.Prokofiev[43] D.Prokofiev[33] J.Quartieri[39] G.Rahal-Callot[46] M.A.Rahaman[10] P.Raics[16] N.Raja[10] R.Ramelli[46] P.G.Rancoita[26] R.Ranieri[17] A.Raspereza[45] P.Razis[29] D.Ren[46] M.Rescigno[38] S.Reucroft[11] S.Riemann[45] K.Riles[3] B.P.Roe[3] L.Romero[24] A.Rosca[8] S.Rosier-Lees[4] S.Roth[1] C.Rosenbleck[1] B.Roux[30] J.A.Rubio[18] G.Ruggiero[17] H.Rykaczewski[46] A.Sakharov[46] S.Saremi[6] S.Sarkar[38] J.Salicio[18] E.Sanchez[24] M.P.Sanders[30] C.Schäfer[18] V.Schegelsky[33] S.Schmidt-Kaerst[1] D.Schmitz[1] H.Schopper[47] D.J.Schotanus[30] G.Schwering[1] C.Sciacca[28] L.Servoli[32] S.Shevchenko[31] N.Shivarov[41] V.Shoutko[14] E.Shumilov[27] A.Shvorob[31] T.Siedenburg[1] D.Son[42] P.Spillantini[17] M.Steuer[14] D.P.Stickland[36] B.Stoyanov[41] A.Straessner[18] K.Sudhakar[10] G.Sultanov[41] L.Z.Sun[21] S.Sushkov[8] H.Suter[46] J.D.Swain[11] Z.Szillasi[25,¶] X.W.Tang[7] P.Tarjan[16] L.Tauscher[5] L.Taylor[11] B.Tellili[23] D.Teyssier[23] C.Timmermans[30] Samuel C.C.Ting[14] S.M.Ting[14] S.C.Tonwar[10,18] J.Tóth[13] C.Tully[36] K.L.Tung[7] J.Ulbricht[46] E.Valente[38] R.T.Van de Walle[30] V.Veszpremi[25] G.Vesztergombi[13] I.Vetlitsky[27] D.Vicinanza[39] G.Viertel[46] S.Villa[37] M.Vivargent[4] S.Vlachos[5] I.Vodopianov[33] H.Vogel[34] H.Vogt[45] I.Vorobiev[34,27] A.A.Vorobyov[33] M.Wadhwa[5] W.Wallraff[1] X.L.Wang[21] Z.M.Wang[21] M.Weber[1] P.Wienemann[1] H.Wilkens[30] S.Wynhoff[36] L.Xia[31] Z.Z.Xu[21] J.Yamamoto[3] B.Z.Yang[21] C.G.Yang[7] H.J.Yang[3] M.Yang[7] S.C.Yeh[49] An.Zalite[33] Yu.Zalite[33] Z.P.Zhang[21] J.Zhao[21] G.Y.Zhu[7] R.Y.Zhu[31] H.L.Zhuang[7] A.Zichichi[9,18,19] G.Zilizi[25,¶] B.Zimmermann[46] M.Zöller[1]

1 I. Physikalisches Institut, RWTH, D-52056 Aachen, FRG[§]
  III. Physikalisches Institut, RWTH, D-52056 Aachen, FRG[§]
2 National Institute for High Energy Physics, NIKHEF, and University of Amsterdam, NL-1009 DB Amsterdam, The Netherlands
3 University of Michigan, Ann Arbor, MI 48109, USA
4 Laboratoire d'Annecy-le-Vieux de Physique des Particules, LAPP,IN2P3-CNRS, BP 110, F-74941 Annecy-le-Vieux CEDEX, France
5 Institute of Physics, University of Basel, CH-4056 Basel, Switzerland
6 Louisiana State University, Baton Rouge, LA 70803, USA
7 Institute of High Energy Physics, IHEP, 100039 Beijing, China[△]
8 Humboldt University, D-10099 Berlin, FRG[§]
9 University of Bologna and INFN-Sezione di Bologna, I-40126 Bologna, Italy
10 Tata Institute of Fundamental Research, Mumbai (Bombay) 400 005, India
11 Northeastern University, Boston, MA 02115, USA
12 Institute of Atomic Physics and University of Bucharest, R-76900 Bucharest, Romania
13 Central Research Institute for Physics of the Hungarian Academy of Sciences, H-1525 Budapest 114, Hungary[‡]
14 Massachusetts Institute of Technology, Cambridge, MA 02139, USA
15 Panjab University, Chandigarh 160 014, India.
16 KLTE-ATOMKI, H-4010 Debrecen, Hungary[¶]
17 INFN Sezione di Firenze and University of Florence, I-50125 Florence, Italy
18 European Laboratory for Particle Physics, CERN, CH-1211 Geneva 23, Switzerland
19 World Laboratory, FBLJA Project, CH-1211 Geneva 23, Switzerland
20 University of Geneva, CH-1211 Geneva 4, Switzerland
21 Chinese University of Science and Technology, USTC, Hefei, Anhui 230 029, China[△]
22 University of Lausanne, CH-1015 Lausanne, Switzerland
23 Institut de Physique Nucléaire de Lyon, IN2P3-CNRS,Université Claude Bernard, F-69622 Villeurbanne, France
24 Centro de Investigaciones Energéticas, Medioambientales y Tecnológicas, CIEMAT, E-28040 Madrid, Spain[♭]
25 Florida Institute of Technology, Melbourne, FL 32901, USA
26 INFN-Sezione di Milano, I-20133 Milan, Italy
27 Institute of Theoretical and Experimental Physics, ITEP, Moscow, Russia
28 INFN-Sezione di Napoli and University of Naples, I-80125 Naples, Italy
29 Department of Physics, University of Cyprus, Nicosia, Cyprus
30 University of Nijmegen and NIKHEF, NL-6525 ED Nijmegen, The Netherlands
31 California Institute of Technology, Pasadena, CA 91125, USA
32 INFN-Sezione di Perugia and Università Degli Studi di Perugia, I-06100 Perugia, Italy
33 Nuclear Physics Institute, St. Petersburg, Russia
34 Carnegie Mellon University, Pittsburgh, PA 15213, USA
35 INFN-Sezione di Napoli and University of Potenza, I-85100 Potenza, Italy
36 Princeton University, Princeton, NJ 08544, USA
37 University of Californa, Riverside, CA 92521, USA
38 INFN-Sezione di Roma and University of Rome, "La Sapienza", I-00185 Rome, Italy
39 University and INFN, Salerno, I-84100 Salerno, Italy
40 University of California, San Diego, CA 92093, USA
41 Bulgarian Academy of Sciences, Central Lab. of Mechatronics and Instrumentation, BU-1113 Sofia, Bulgaria
42 The Center for High Energy Physics, Kyungpook National University, 702-701 Taegu, Republic of Korea
43 Purdue University, West Lafayette, IN 47907, USA
44 Paul Scherrer Institut, PSI, CH-5232 Villigen, Switzerland
45 DESY, D-15738 Zeuthen, FRG
46 Eidgenössische Technische Hochschule, ETH Zürich, CH-8093 Zürich, Switzerland
47 University of Hamburg, D-22761 Hamburg, FRG
48 National Central University, Chung-Li, Taiwan, China
49 Department of Physics, National Tsing Hua University, Taiwan, China
§ Supported by the German Bundesministerium für Bildung, Wissenschaft, Forschung und Technologie
‡ Supported by the Hungarian OTKA fund under contract numbers T019181, F023259 and T024011.
¶ Also supported by the Hungarian OTKA fund under contract number T026178.
♭ Supported also by the Comisión Interministerial de Ciencia y Tecnología.
♯ Also supported by CONICET and Universidad Nacional de La Plata, CC 67, 1900 La Plata, Argentina.
△ Supported by the National Natural Science Foundation of China.

Channel	$(K^-\pi^+)\pi_s^+$	$(K^-\pi^+\pi^0)\pi_s^+$	$(K^-\pi^+\pi^-\pi^+)\pi_s^+$
$N_{obs}^{D^{*\pm}}$	245 ± 27	139 ± 18	99 ± 16
ε_{trig}, %	92.9 ± 0.2	92.1 ± 0.3	89.4 ± 0.2
$\varepsilon_{vis}^{D^{*\pm}}$, %	0.61 ± 0.03	0.22 ± 0.02	0.20 ± 0.02
$\sigma_{vis}^{D^{*\pm}}$, pb	$63.3 \pm 6.7 \pm 8.9$	$100.9 \pm 13.0 \pm 18.2$	$81.1 \pm 12.5 \pm 17.8$
$\sigma(e^+e^- \to e^+e^- c\bar{c}X)$, nb	$1.00 \pm 0.11 \pm 0.15^{+0.48}_{-0.22}$	$1.59 \pm 0.21 \pm 0.31^{+0.77}_{-0.36}$	$1.28 \pm 0.20 \pm 0.29^{+0.62}_{-0.29}$

Table 1: The number of observed $D^{*\pm}$ mesons for the three different channels and the trigger (ε_{trig}) and visible ($\varepsilon_{vis}^{D^{*\pm}}$) efficiencies. Visible and total cross sections are also given. The uncertainties on the numbers of reconstructed $D^{*\pm}$ mesons and on the efficiencies are statistical. For the cross section values, the first uncertainty is statistical, the second is systematic. The last uncertainty for the total charm cross section corresponds to the extrapolation to the total phase space.

| P_T(GeV)	$N_{obs}^{D^{*\pm}}$	$d\sigma/dP_T$ (pb/GeV)	$\Delta\sigma$ (pb)
$1 - 2$	325 ± 31	$54.5 \pm 5.3 \pm 6.7$	$54.5 \pm 5.3 \pm 6.7$
$2 - 3$	130 ± 17	$12.1 \pm 1.4 \pm 1.4$	$12.1 \pm 1.4 \pm 1.4$
$3 - 5$	72 ± 11	$2.9 \pm 0.4 \pm 0.4$	$6.7 \pm 1.0 \pm 1.0$
$5 - 12$	13 ± 5	$0.12 \pm 0.05 \pm 0.02$	$1.5 \pm 0.6 \pm 0.3$

Table 2: Number of observed $D^{*\pm}$ mesons $N_{obs}^{D^{*\pm}}$ and measured $D^{*\pm}$ production cross sections in different P_T bins for $|\eta| < 1.4$. Differential $d\sigma/dP_T$ cross sections refer to the center of the bin and $\Delta\sigma$ is the integral over the bin.

$|\eta|$	$N_{obs}^{D^{*\pm}}$	$d\sigma/d|\eta|$ (pb)	$\Delta\sigma$ (pb)
$0.0 - 0.4$	194 ± 23	$49.4 \pm 6.0 \pm 6.0$	$19.8 \pm 2.4 \pm 2.4$
$0.4 - 0.8$	232 ± 24	$60.3 \pm 6.0 \pm 7.2$	$24.1 \pm 2.4 \pm 2.9$
$0.8 - 1.4$	92 ± 17	$39.4 \pm 7.2 \pm 5.6$	$23.6 \pm 4.3 \pm 3.4$

Table 3: Number of observed $D^{*\pm}$ mesons $N_{obs}^{D^{*\pm}}$ and measured $D^{*\pm}$ production cross sections for 1 GeV $< P_T <$ 12 GeV. Differential $d\sigma/d|\eta|$ cross sections refer to the center of the bin and $\Delta\sigma$ is the integral over the bin.

Source	$(K^-\pi^+)\pi_s^+$	$(K^-\pi^+\pi^0)\pi_s^+$	$(K^-\pi^+\pi^-\pi^+)\pi_s^+$
Selection	7.8	9.9	16.8
Branching Ratio [14]	3.1	7.2	4.9
Fit procedure	6.6	6.6	6.6
Direct/Resolved ratio	8.6	8.6	8.6
Monte Carlo statistics	5.1	9.4	8.7
Trigger efficiency	0.2	0.3	0.2
Systematics visible	14.6	18.9	22.3
$P(c \rightarrow D^{*+})$	3.1	3.1	3.1
$b\bar{b}$ contribution	0.6	0.6	0.6
Systematics total	14.9	19.2	22.5

Table 4: Sources of systematic uncertainty in % on the visible $D^{*\pm}$ cross section and the total charm cross section. The total systematic uncertainty is calculated by adding all contributions in quadrature.
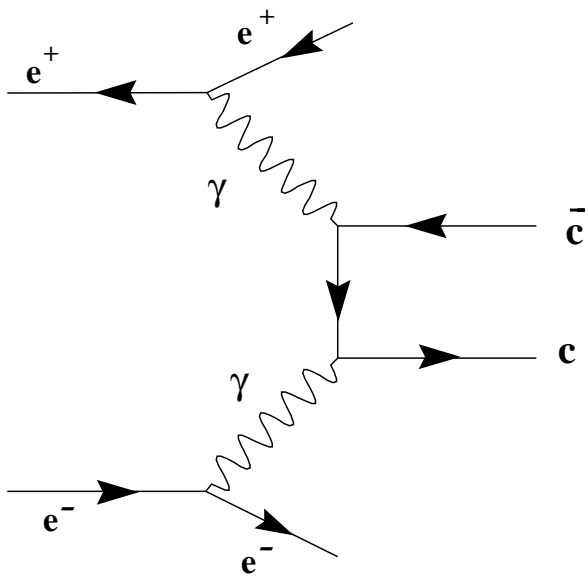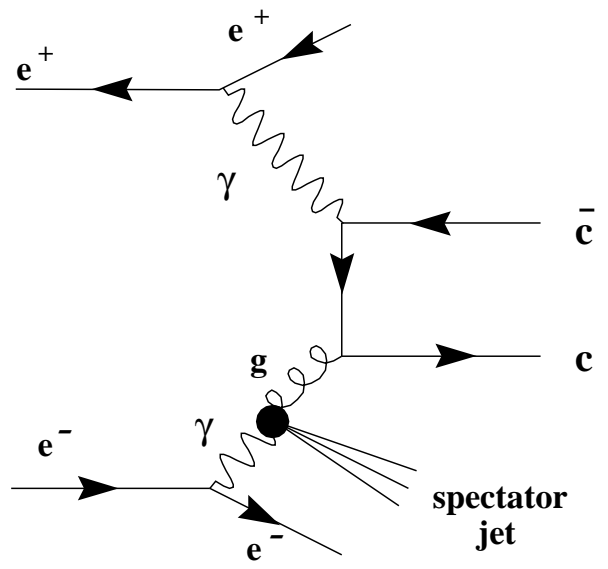
Direct   **Single Resolved**

Figure 1: Diagrams contributing to charm production in $\gamma\gamma$ collisions.
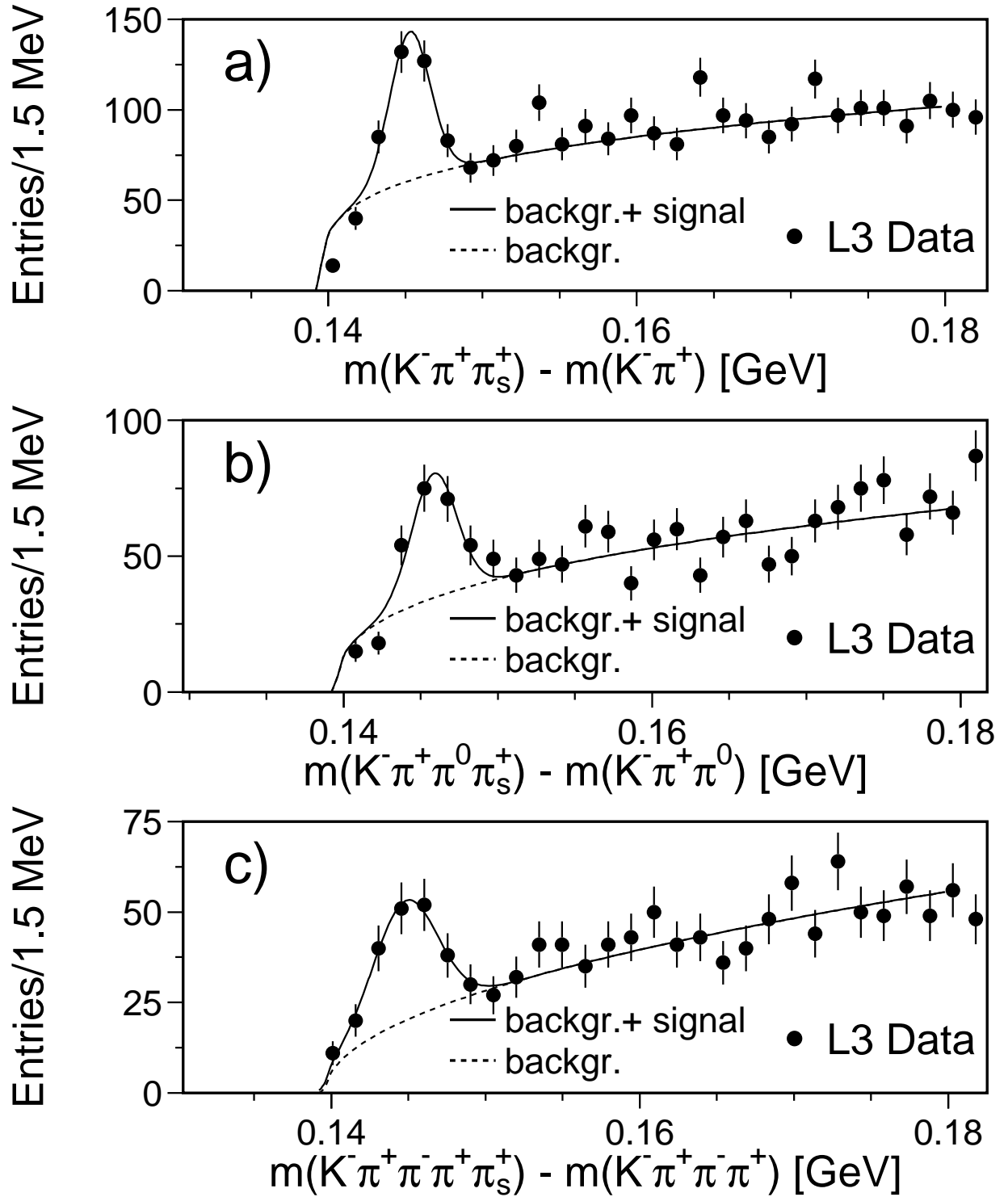
Figure 2: Distribution of the mass difference D^{*+} and D^0 candidates for D^{*+} decays into a) $(K^-\pi^+)\pi_s^+$, b) $(K^-\pi^+\pi^0)\pi_s^+$ and c) $(K^-\pi^+\pi^-\pi^+)\pi_s^+$. The points are data, the error bars represent statistical uncertainties and the line is the result of the fit to the data points.
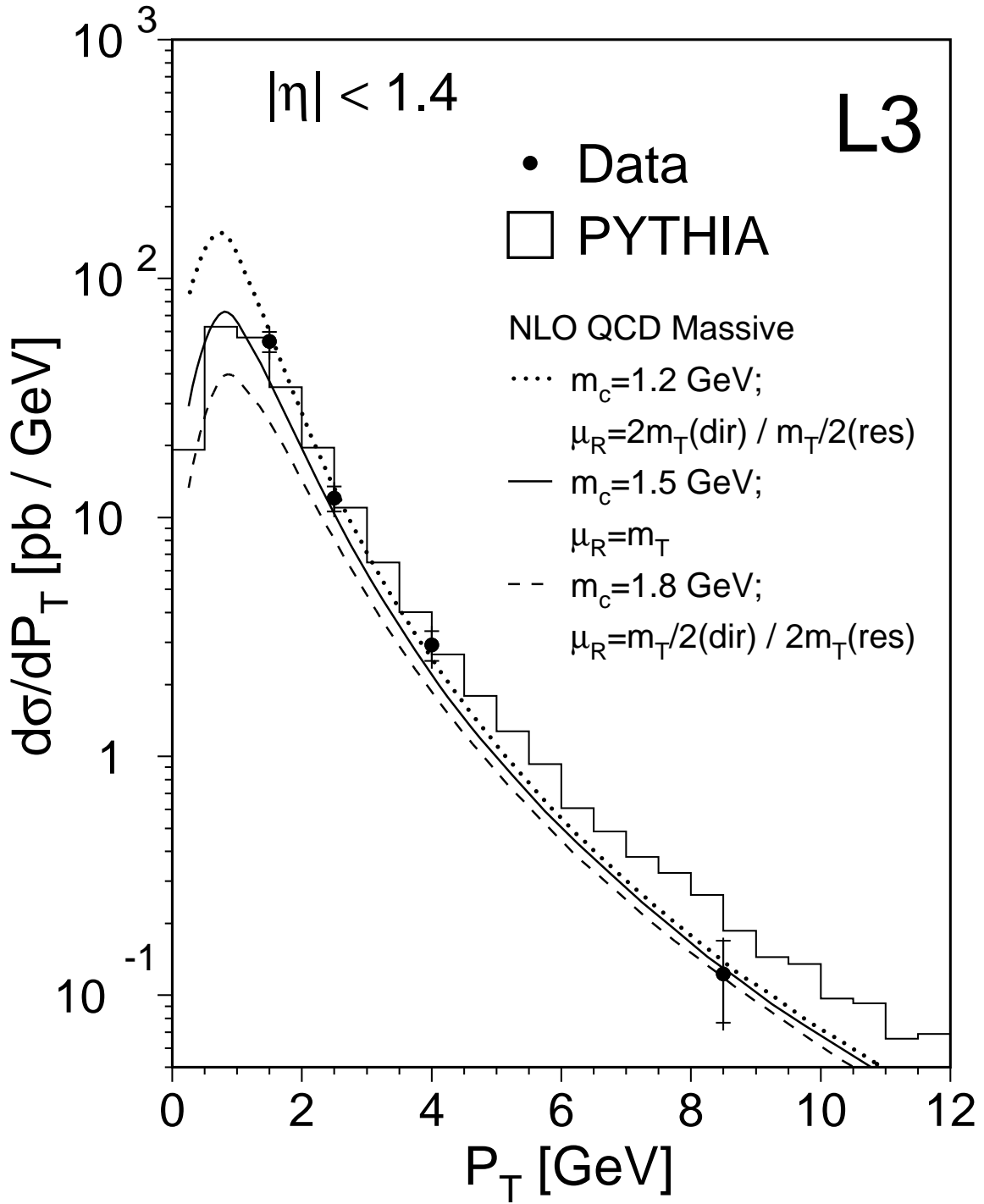
Figure 3: The differential cross section $d\sigma/dP_T$ for inclusive $\text{D}^{*\pm}$ production. The points are the data, the inner error bars represent the statistical uncertainty. The solid curve represents the NLO QCD calculations [15] with the Glück-Reya-Schienbein [16] parametrization of the parton density of the photon. For the direct (dir) and resolved (res) processes, different values of the renormalisation and factorisation scales μ_R and μ_F, as well as of m_c, are used. The PYTHIA prediction is shown as a histogram.
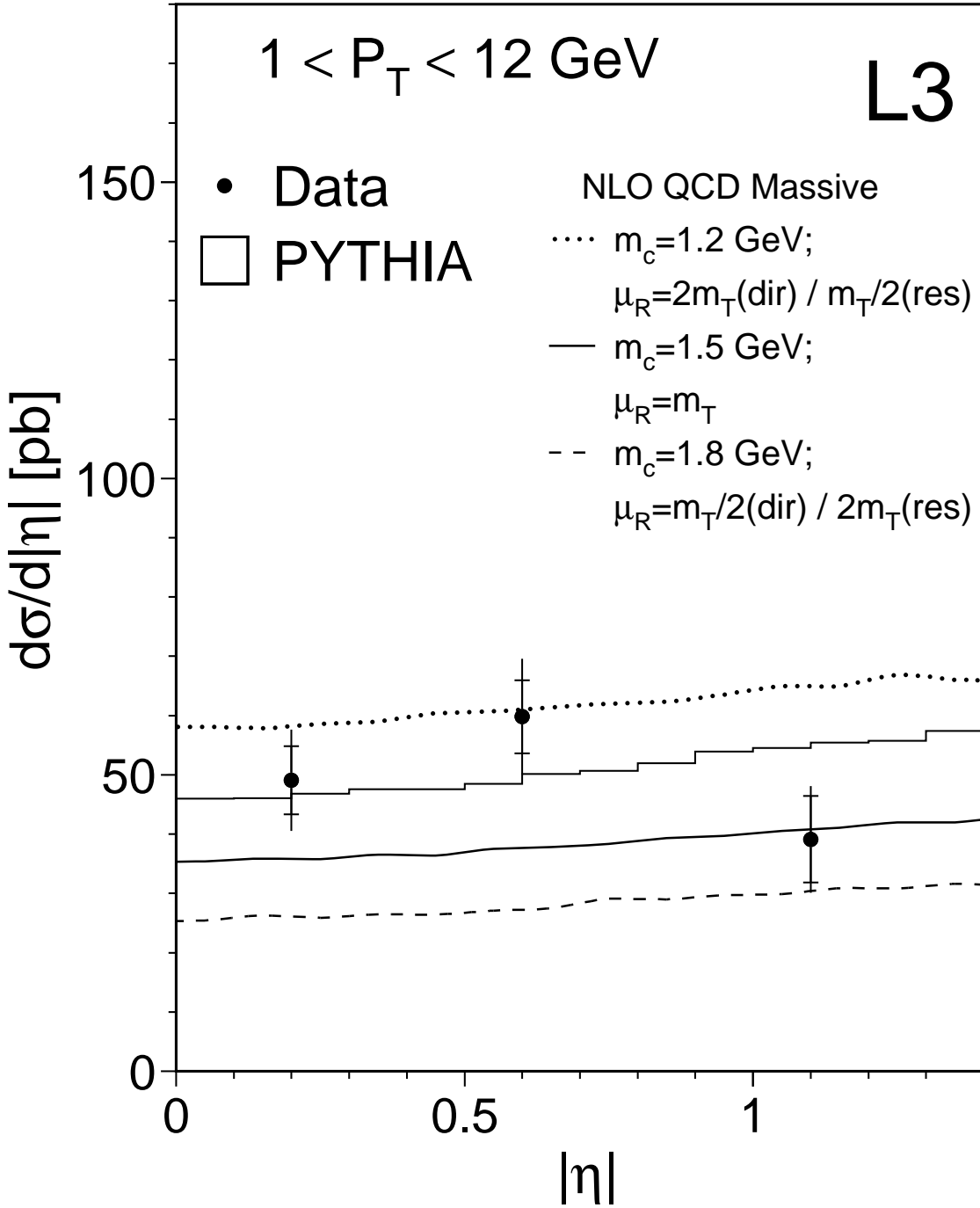
Figure 4: The differential cross section $d\sigma/d|\eta|$ for inclusive $D^{*\pm}$ production. The points are the data, the inner error bars represent the statistical uncertainty. The solid curve represents the NLO QCD calculations [15] with the Glück-Reya-Schienbein [16] parametrization of the parton density of the photon. For the direct (dir) and resolved (res) processes, different values of the renormalisation and factorisation scales μ_R and μ_F, as well as of m_c, are used. The PYTHIA prediction is shown as a histogram.
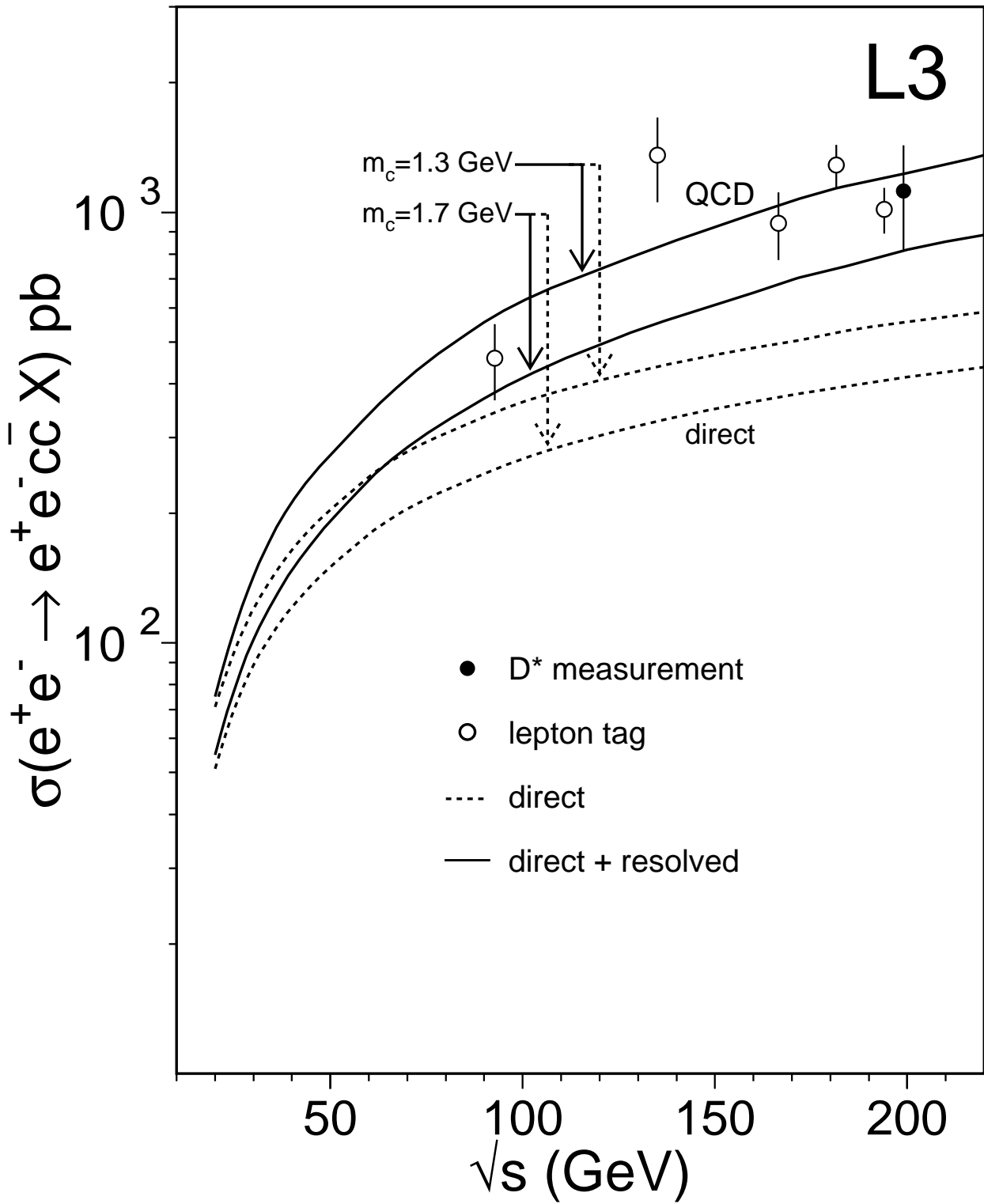
Figure 5: The open charm production cross section in two-photon collisions as a function of the e⁺e⁻ centre-of-mass energy. L3 measurements based on lepton tag [6, 8] are plotted as the open circles. The dashed lines correspond to the direct process contribution and the solid lines represent the NLO QCD prediction [1] for the sum of the direct and resolved processes. The effect of different values of m_c is also shown.